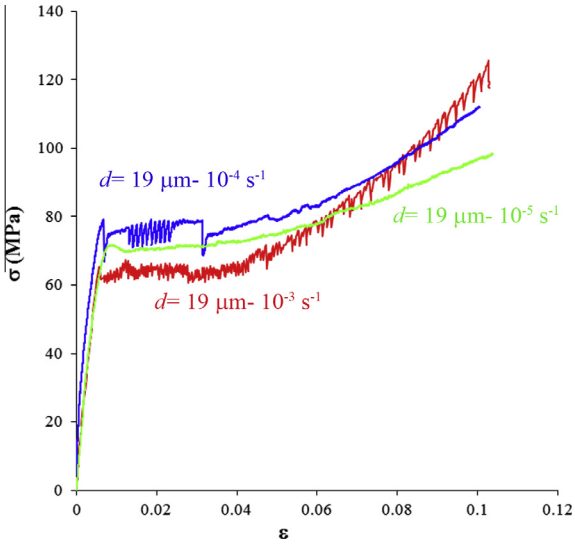

Fig. 8. Compressive true stress–true strain curves corresponding to the pure Mg polycrystal with $d = 19$ μm deformed at 50 °C and at initial strain rates of 10^{-3}, 10^{-4} and 10^{-5} s^{-1}.

fraction of "well-connected" clusters of grains favorably oriented for basal slip in the fine grained microstructures. It must be emphasized here that in a large majority of the studies aimed to analyze the influence of grain size on the mechanical behavior of Mg alloys [5–18,20–23,43,51–54] the samples with different d values are first processed by rolling or extrusion at moderate to elevated temperatures to avoid cracking, and then annealed to reach the desired average grain size value. Unavoidably, these processing routes lead to well known deformation textures, which have been exhaustively characterized [5]. To our knowledge, however, no studies in the past have quantified the correlations between the rolling and extrusion processing parameters and the percolation properties of the resulting GB networks in pure Mg and in Mg alloys. Nevertheless, it is known that clusters of grains well oriented for basal slip do form during rolling and extrusion of Mg alloys at low to moderate temperatures [55–57], while subsequent annealing at higher temperatures leads to the preferential growth of grains with c-axes parallel to the rolling plane or, respectively, perpendicular to the extrusion direction. Thus, it seems logical to presume that the connectivity of the clusters of grains favorably oriented for basal slip decreases with increasing d in most of the works in which polycrystals were processed using these conventional processing routes, as demonstrated in the present study.

3.2. Twinning to slip transition with decreasing strain rate

Fig. 8 shows the compression true stress–strain curves corresponding to the pure Mg polycrystal with $d = 19$ μm tested at 50 °C and at initial strain rates of 10^{-3}, 10^{-4} and 10^{-5} s^{-1}. In general, the three curves exhibit a plateau after yielding, followed by different levels of work hardening, the latter decreasing as the strain rate is reduced. In addition, the curves corresponding to strain rates of 10^{-3} and 10^{-4} s^{-1} exhibit serrations, which are typically attributed to nucleation and propagation of twinning Lüders bands (Fig. 2) [1]. However, such serrated flow is absent from the curve corresponding to the lowest strain rate, suggesting a transition from twinning to slip dominated flow.

Fig. 9 illustrates several representative SEM micrographs corresponding to the same polycrystal after compression at 50 °C and at 10^{-4} s^{-1} (Fig. 9a) and 10^{-5} s^{-1} (Fig. 9b). Comparison of Fig. 9 with Fig. 2 allows analyzing the microstructural influence of strain rate on the microstructural evolution during straining. While at the highest strain rate twinning was clearly the dominant deformation mechanism (Fig. 2), when the strain rate is reduced down to 10^{-4} s^{-1}, both twinning and slip are apparent (Fig. 9a). At 10^{-5} s^{-1} (Fig. 9b) intense slip localization takes place along deformation bands. Out of the 119 slip traces analyzed in the polycrystal after compression at 10^{-5} s^{-1}, 91% corresponded to basal slip, 6% to prismatic ⟨a⟩ slip, and 3% to pyramidal ⟨c+a⟩ slip. At this strain rate the fraction of twinned grains is very low (8%), as observed in the corresponding EBSD IPF map after deformation (Fig. 10). Thus, these results evidence again a clear transition from twinning to basal slip dominated flow as the strain rate decreases from 10^{-3} to 10^{-5} s^{-1} in the pure Mg polycrystal with $d = 19$ μm.

Fig. 11a illustrates the misorientation distribution histogram corresponding to GBs located within the deformation bands developed at 10^{-5} s^{-1} in the pure Mg polycrystal with $d = 19$ μm. GBs allowing slip transfer (blue) and arresting slip (red) are differentiated. It can be seen that θ_{th} increased from 30° at 10^{-3} s^{-1} (Fig. 4) to 45° at 10^{-5} s^{-1}. This is consistent with a relaxation of constraints

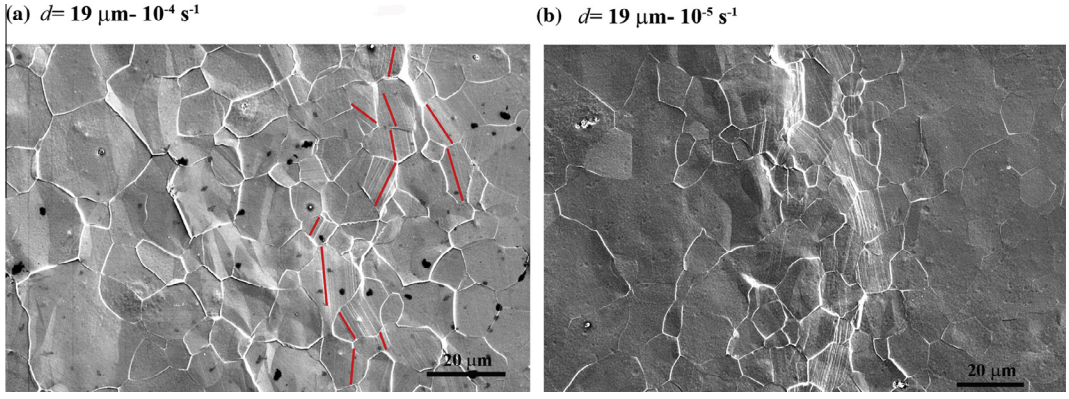

Fig. 9. SEM micrographs illustrating the microstructure of the polycrystal with $d = 19$ μm after compression at 50 °C at: (a) 10^{-4} s^{-1} and (b) 10^{-5} s^{-1}.